Structural Insights into the Polymorphism of Amyloid-Like Fibrils Formed by Region 20-29 of Amylin Revealed by Solid-State NMR and X-ray Fiber Diffraction

ARTICLE *in* JOURNAL OF THE AMERICAN CHEMICAL SOCIETY · NOVEMBER 2008

Impact Factor: 12.11 · DOI: 10.1021/ja802483d · Source: PubMed

6 AUTHORS, INCLUDING:

Jillian Madine
University of Liverpool
27 PUBLICATIONS **370** CITATIONS
SEE PROFILE

Sheena E Radford
University of Leeds
270 PUBLICATIONS **15,955** CITATIONS
SEE PROFILE

J|A|C|S
ARTICLES

Published on Web 10/21/2008

Structural Insights into the Polymorphism of Amyloid-Like Fibrils Formed by Region 20−29 of Amylin Revealed by Solid-State NMR and X-ray Fiber Diffraction

Jillian Madine,[†] Edward Jack,[‡] Peter G. Stockley,[§] Sheena E. Radford,[§] Louise C. Serpell,[||] and David A. Middleton*[,†]

School of Biological Sciences, University of Liverpool, Crown Street, Liverpool L69 7ZB, U.K., Faculty of Life Sciences, University of Manchester, Manchester M60 1QD, U.K., Astbury Centre for Structural Molecular Biology, University of Leeds, Leeds LS2 9JT, U.K., and Department of Biochemistry, School of Life Sciences, University of Sussex, Falmer, Brighton BN1 9QG, U.K.

Received April 13, 2008; E-mail: middleda@liv.ac.uk

Abstract: Many unrelated proteins and peptides can assemble into amyloid or amyloid-like nanostructures, all of which share the cross-β motif of repeat arrays of β-strands hydrogen-bonded along the fibril axis. Yet, paradoxically, structurally polymorphic fibrils may derive from the same initial polypeptide sequence. Here, solid-state nuclear magnetic resonance (SSNMR) analysis of amyloid-like fibrils of the peptide hIAPP$_{20-29}$, corresponding to the region S^{20}NNFGAILSS^{29} of the human islet amyloid polypeptide amylin, reveals that the peptide assembles into two amyloid-like forms, (1) and (2), which have distinct structures at the molecular level. Rotational resonance SSNMR measurements of ^{13}C dipolar couplings between backbone F23 and I26 of hIAPP$_{20-29}$ fibrils are consistent with form (1) having parallel β-strands and form (2) having antiparallel strands within the β-sheet layers of the protofilament units. Seeding hIAPP$_{20-29}$ with structurally homogeneous fibrils from a 30-residue amylin fragment (hIAPP$_{8-37}$) produces morphologically homogeneous fibrils with similar NMR properties to form (1). A model for the architecture of the seeded fibrils is presented, based on the analysis of X-ray fiber diffraction data, combined with an extensive range of SSNMR constraints including chemical shifts, torsional angles, and interatomic distances. The model features a cross-β spine comprising two β-sheets with an interface defined by residues F23, A25, and L27, which form a hydrophobic zipper. We suggest that the energies of formation for fibril form containing antiparallel and parallel β-strands are similar when both configurations can be stabilized by a core of hydrophobic contacts, which has implications for the relationship between amino acid sequence and amyloid polymorphism in general.

Introduction

Many natural and designed peptides and proteins assemble into amyloid fibril assemblies consisting of β-strands arranged with the interstrand hydrogen bonds parallel to the fibril long axis in a repeat array known as a cross-β structure.[1] Mature fibrils are typically ~10 nm in diameter, long, and unbranched and are usually formed from simpler units known as protofilaments. Recent crystallography from microcrystals of short amyloidogenic peptide fragments indicate that protofilaments consist of a common cross-β spine formed by a minimum of two β-sheet layers.[2] The two layers can pack together with interdigitated side groups forming a steric zipper with "wet" and "dry" interfaces.[3] Solid state nuclear magnetic resonance (SSNMR) is a valuable complementary technique to X-ray diffraction which has provided detailed models of amyloid fibrils formed by peptide fragments, for example from Aβ_{1-40}, β_2-microglobulin, and transthyretin,[4−6] as well as constraints on the protein structure and architecture of fibrils formed from α-synuclein,[7] amylin,[8] and the fungal prion HetS.[9]

Recent research into the sequential and structural determinants of protein aggregation is beginning to shed light on how chemically diverse molecules can form amyloid fibrils with a common cross-β structure and morphology. Paradoxically, it is also becoming clear that amyloid fibril assemblies with diverse morphologies or molecular architectures can grow from the same

[†] University of Liverpool.
[‡] University of Manchester.
[§] University of Leeds.
[||] University of Sussex.

(1) Gazit, E. *FEBS J.* **2005**, *272*, 5971.
(2) Nelson, R.; Sawaya, M. R.; Balbirnie, M.; Madsen, A. O.; Riekel, C.; Grothe, R.; Eisenberg, D. *Nature* **2005**, *435*, 773.
(3) Sawaya, M. R.; Sambashivan, S.; Nelson, R.; Ivanova, M. I.; Sievers, S. A.; Apostol, M. I.; Thompson, M. J.; Balbirnie, M.; Wiltzius, J. J. W.; McFarlane, H. T.; Madsen, A. O.; Riekel, C.; Eisenberg, D. *Nature* **2007**, *447*, 453.
(4) Petkova, A. T.; Ishii, Y.; Balbach, J. J.; Antzutkin, O. N.; Leapman, R. D.; Delaglio, F.; Tycko, R. *Proc. Natl. Acad. Sci. U.S.A.* **2002**, *99*, 16742.
(5) van der Wel, P. C. A.; Lewandowski, J. R.; Griffin, R. G. *J. Am. Chem. Soc.* **2007**, *129*, 5117.
(6) Iwata, K.; Fujiwara, T.; Matsuki, Y.; Akutsu, H.; Takahashi, S.; Naiki, H.; Goto, Y. *Proc. Natl. Acad. Sci. U.S.A.* **2006**, *103*, 18119.
(7) Heise, H.; Hoyer, W.; Becker, S.; Andronesi, O. C.; Riedel, D.; Baldus, M. *Proc. Natl. Acad. Sci. U.S.A.* **2005**, *102*, 15871.
(8) Luca, S.; Yau, W.-M.; Leapman, R. D.; Tycko, R. *Biochemistry* **2007**, *46*, 13505.
(9) Wasmer, C.; Lange, A.; van Melckebeke, H.; Siemer, A. B.; Riek, R.; Meier, B. H. *Science* **2008**, *319*, 1521.

10.1021/ja802483d CCC: $40.75

initial polypeptide sequence.[10−15] The structural basis for amyloid polymorphism may originate from differences in the secondary, tertiary, and/or quaternary structure of the polypeptide molecules, or in the way that protofilament units associate laterally.[12] For example, the Lewy body-associated protein α-synuclein forms two types of fibrils which differ in the distribution of hydrogen bonded β-strands.[7] Multiple morphologies or structures can propagate simultaneously, or individual morphologies can be promoted by specific growth conditions (temperature, pH) or manipulated by small molecules. Specific "daughter" fibril morphologies of Aβ polypeptides associated with Alzheimer's disease have been produced selectively by seeding with structurally homogeneous "parent" seeds,[14] which may have implications for different strains and form barriers shown by prion proteins, for example.

Pancreatic amyloid deposits, present in the vast majority of type II diabetes patients, are formed by the aggregation of the 37-aa human islet amyloid polypeptide (hIAPP) also known as amylin.[16] Recent SSNMR measurements of amylin fibrils by Tycko and co-workers have provided several constraints on the peptide secondary and tertiary structure within fibrils having a striated ribbon morphology, although a complete, unambiguous high-resolution structure has yet to be determined.[8] Residues 20−29 of hIAPP form part of the amyloidogenic core and can assemble into fibrils independently of the full-length polypeptide, whereas the flanking C- and N-terminal regions of the peptide may determine the interactions involved in the formation of higher order coiled polymorphic superstructures.[17,18] The atomic structure obtained from microcrystals of the segment NNFGAIL (residues 21−27 of hIAPP) reveals an unusual packing of β-sheet layers, which contain a bend facilitated by the central glycine allowing a tight (∼3 Å) main-chain interface between F, G, and A of opposing sheets.[19] The shorter peptide segments NFGAIL and FGAIL also form β-sheet containing fibrils but aggregate into completely different fibrillar assemblies, thus highlighting the significant morphological variability that occurs in this region.[20]

Here, SSNMR has been used to characterize the amyloid-like fibrils formed by the peptide AcNH-SNNFGAILSS-$CONH_2$ ($hIAPP_{20-29}$) constituting residues 20−29 of amylin. Earlier FTIR studies of aggregates of this peptide suggested a crude model of the fibrils with antiparallel β-strands aligned with the GAIL sequence in-register (i.e., with A25 hydrogen bonded to I26), although subsequent SSNMR studies suggested a more complex antiparallel alignment.[21,22] Here, high resolution ^{13}C SSNMR spectra reveal that the fibrils are morphologically heterogeneous and consist of two distinct forms or domains which differ in the alignment of hydrogen bonded peptide molecules. It is shown that one of the forms occurs exclusively when aggregation is heterologously seeded by morphologically uniform fibrils of a 30-aa peptide fragment of amylin ($hIAPP_{8-37}$) known to exhibit all the hallmarks of amyloid formed by full-length (37 aa) amylin.[18] By combining an extensive ensemble of structural constraints measured using SSNMR with studies of the same fibrils using X-ray fiber diffraction, we propose a model for the cross-β spine of the seeded $hIAPP_{20-29}$ fibrils and discuss the consequences of these observations for the formation and selective propagation of polymorphic structures of amyloid in general.

Table 1. Summary of the Nomenclature for the ^{13}C and ^{15}N Labelled Peptides Used in This Work and the Figures in Which They Appear[a]

name	labeling pattern	experiments
[U-^{13}C,^{15}N-FGAI]$hIAPP_{20-29}$	SNN**FGAI**LSS	Figures 1, 3, 5
[C′-^{13}C-F23]$hIAPP_{20-29}$	SNN**F(C′)**GAILSS	Figure 2
[C′-^{13}C-I26]$hIAPP_{20-29}$	SNNFGA**I(C′)**LSS	Figure 2
[α-^{13}C-F23]$hIAPP_{20-29}$	SNN**F(Cα)**GAILSS	Figures 2, 3
[U-^{13}C,^{15}N-N21/S28]$hIAPP_{20-29}$	S**N**NFGAIL**S**S	Figure 4
[U-^{13}C,^{15}N-SNNF]$hIAPP_{20-29}$	**SNNF**GAILSS	Figure 5
[β-^{13}C-A]$hIAPP_{20-29}$	SNNFG**A(Cβ)**ILSS	Figure 5
[U-^{13}C,^{15}N-ILSS]$hIAPP_{20-29}$	SNNFGA**ILSS**	Figures 5, 6, 7
[U-^{13}C,^{15}N-L27]$hIAPP_{20-29}$	SNNFGAI**L**SS	Figure 9

[a] Labelled residues are underlined. "U" denotes uniformly labelled, and C′ denotes the carbonyl carbon. All peptides were N-acetylated and C-terminally amidated.

Experimental Section

General. Synthetic $hIAPP_{20-29}$ and $hIAPP_{8-37}$ were purchased from Peptide Protein Research (U.K.) Ltd. The various labeling patterns for the peptides are summarized in Table 1. Fibrils of $hIAPP_{20-29}$ were prepared essentially as described elsewhere.[17,18,23] Briefly, the peptides were dissolved in DMSO and sonicated for 3 min to ensure that any aggregates were broken down into monomers. The peptide solution in DMSO was then added to 10 mM phosphate, pH 7.4, to a final DMSO concentration of 1% v/v and a peptide concentration of 1 mM. The solution was incubated with agitation at room temperature without seeding for 4 d or for 1 d after adding 2 μL of seed to 1 mL of incubation solution. Fibrils were harvested by spinning down in a benchtop centrifuge for 30 min. Seeds were prepared by sonicating preformed $hIAPP_{8-37}$ fibrils in DMSO. Models were visualized using PyMOL (DeLano Scientific LLC) and were created without energy minimization or further refinement.

Solid-State NMR Experiments. All NMR experiments were performed on hydrated fibrils using a Bruker Avance 400 spectrometer operating at a magnetic field of 9.3 T. Experiments were carried out at −10 °C to reduce interference from molecular dynamics and with cross-polarization magic-angle spinning (CP-MAS) to obtain high-resolution spectra. Samples were packed into a 4 mm zirconium rotor and rotated at the magic angle at rates between 4 and 13 kHz, while maintaining the spinning rate automatically to within ±1 Hz. All experiments utilized an initial 4.0-μs ^1H 90° excitation pulse length, 1-ms Hartmann−Hahn contact time at a matched ^1H field of 65 kHz, TPPM proton

(10) Dzwolak, W.; Smirnovas, V.; Jansen, R.; Winter, R. *Protein Sci.* **2004**, *13*, 1927.
(11) Gordon, D. J.; Balbach, J. J.; Tycko, R.; Meredith, S. C. *Biophys. J.* **2004**, *86*, 428.
(12) Kodali, R.; Wetzel, R. *Curr. Opin. Struct. Biol.* **2007**, *17*, 48.
(13) Paravastu, A. K.; Petkova, A. T.; Tycko, R. *Biophys. J.* **2006**, *90*, 4618.
(14) Petkova, A. T.; Leapman, R. D.; Guo, Z. H.; Yau, W. M.; Mattson, M. P.; Tycko, R. *Science* **2005**, *307*, 262.
(15) Pedersen, J. S.; Otzen, D. E. *Protein Sci.* **2008**, *17*, 2.
(16) Hoppener, J. W. M.; Lips, C. J. M. *Int. J. Biochem. Cell Biol.* **2006**, *38*, 726.
(17) Goldsbury, C.; Goldie, K.; Pellaud, J.; Seelig, J.; Frey, P.; Muller, S. A.; Kistler, J.; Cooper, G. J. S.; Aebi, U. *J. Struct. Biol.* **2000**, *130*, 352.
(18) Westermark, P.; Engstrom, U.; Johnson, K. H.; Westermark, G. T.; Betsholtz, C. *Proc. Natl. Acad. Sci. U.S.A.* **1990**, *87*, 5036.
(19) Wiltzius, J. J. W.; Sievers, S. A.; Sawaya, M. R.; Cascio, D.; Popov, D.; Riekel, C.; Eisenberg, D. *Protein Sci.* **2008**, in press.
(20) Tenidis, K.; Waldner, M.; Bernhagen, J.; Fischle, W.; Bergmann, M.; Weber, M.; Merkle, M. L.; Voelter, W.; Brunner, H.; Kapurniotu, A. *J. Mol. Biol.* **2000**, *295*, 1055.
(21) Ashburn, T. T.; Auger, M.; Lansbury, P. T. *J. Am. Chem. Soc.* **1992**, *114*, 790.
(22) Griffiths, J. M.; Ashburn, T. T.; Auger, M.; Costa, P. R.; Griffin, R. G.; Lansbury, P. T. *J. Am. Chem. Soc.* **1995**, *117*, 3539.
(23) Jack, E.; Newsome, M.; Stockley, P. G.; Radford, S. E.; Middleton, D. A. *J. Am. Chem. Soc.* **2006**, *128*, 8098.

decoupling[24] at a field of 85 kHz during signal acquisition, and a 2-s recycle delay.

Multiple quantum (MQ) ^{13}C NMR spectra were obtained using the time-reversible pulse sequence with an initial condition of longitudinal ^{13}C spin polarization (i.e., 2-quantum selective) described by Antzutkin and Tycko.[25] The data were processed to give a series of spectra representing the probability of exciting and detecting even orders of quantum coherences.[25] The excitation/preparation periods were adjusted to 14.4 ms and a train of 8-μs π pulses were applied at the ^{13}C frequency during these periods to refocus chemical shift evolution. A series of 32 spectra were acquired with phase incrementation, each from the accumulation of 10 240 scans and processed with cosine Fourier transformation to obtain the MQ profile.

Dipolar assisted rotational resonance (DARR) spectra[26] were recorded with 256 hypercomplex points in the indirect dimension (unless stated otherwise), with mixing times between 1 and 200 ms during which the proton field was adjusted to a spinning frequency of 8 kHz. Experiments to determine the backbone conformation of the hIAPP$_{20-29}$ peptide molecules within the fibrils were carried out using block-wise isotope labeled peptides[27] to reduce spectral overcrowding. Backbone ϕ and Ψ torsional angles were estimated from ^{13}C and ^{15}N shifts[28] and measured directly in NMR experiments to determine the relative orientations of N−H and C−H bonds.[29,30] These experiments were performed at a sample spinning rate of 6000 Hz, with 64 increments in t_1. Side group conformations were measured using ^{13}C-observe, ^{15}N-dephase REDOR at a spinning rate of 8 kHz by applying a train of 16-μs π pulses at the ^{15}N frequency every half-rotor period during the dephasing interval and a 8-μs π pulse at the ^{13}C frequency in the center of the dephasing interval.[31] Rotational resonance (RR) experiments were carried out by adjusting the sample spinning rate (ω_R) to the difference between the Cα and C′ resonance frequencies ($\Delta\Omega$) for F23 or for Cα of F23 and C′ of I26 (i.e., the $n = 1$ rotational resonance condition). After cross-polarization, ^{13}C longitudinal difference polarization was created with a nonselective 4-μs $\pi/2$ pulse followed by a train of 18 DANTE pulses, representing an overall π pulse of 30 μs, to invert the ^{13}C spin polarization for Cα selectively. After a mixing period the ^{13}C magnetization was returned to the transverse plane by a second nonselective $\pi/2$ pulse before digitization of the free-induction decay. A series of experiments using mixing periods of up to 50 ms was performed to measure the time dependence of difference polarization. Curves representing exchange of Zeeman order were obtained from the difference in intensities for the Cα and C′ peaks. Peak intensities were adjusted so as to take into account the population of labeled peptides in excess that did not contribute to the RR effect.

Numerical Simulations of Magnetization Exchange Curves. Simulation of magnetization exchange between C′ and Cα spins at $n = 1$ RR were carried out with a Fortran computer program written specifically for that purpose. Curves were calculated as a function of the distance-dependent ^{13}C−^{13}C dipolar coupling constant d_{cc} and the zero quantum relaxation time T_2^{ZQ}, as described elsewhere.[32] The value of T_2^{ZQ} can dominate the shape of the magnetization curve when the dipolar coupling is weak and so must be included in the simulations. The similarity between the curves and the experimental data was quantified by determining χ^2 for each curve. In practice a series of curves were calculated for different combinations of d_{cc} and T_2^{ZQ} to produce a χ^2 matrix, in which the minimum values corresponded to the curves in closest agreement with the experimental data. The lower limit of T_2^{ZQ} used in these simulations was estimated from the off-RR line widths at half-height for the two spins (L_1 and L_2) according to

$$T_2^{ZQ} = \frac{1}{\pi(L_1 + L_2)}$$

Values for chemical shift anisotropy and asymmetry parameters were measured from the solid amino acids leucine and phenylalanine. Also required in the simulation are the Euler angles defining the relative orientations of the chemical shielding and dipolar tensors. This orientational information could not be determined without having prior knowledge of the molecular packing geometry of the fibrils. At $n = 1$ RR, however, the tensor orientations have a negligible effect on the magnetization exchange curves and simulations covering the full range of Euler angle combinations (all other parameters being constant) confirmed that the maximum variation between exchange curves was less than 0.07 units at up to a mixing period of 50 ms. Values of d_{cc} giving the lowest χ^2 values were translated into internuclear distances.[32]

X-ray Diffraction. A droplet of solution of seeded amyloid fibrils of hIAPP$_{20-29}$ was placed between two wax filled capillary tubes on a stretch frame, and the fibrils were allowed to dry to form a partially aligned fiber sample as previously described.[33] X-ray diffraction data were collected using a Rigaku rotating anode (CuKalpha) and RAxis 4++ detector with a specimen-to-detector distance of 160 mm and exposure times of 10−20 min. X-ray diffraction patterns were examined using a computer program called CLEARER. Positions of diffraction signals were measured and potential unit cell dimensions were explored using the unit cell determination algorithm within CLEARER. Constraints from SSNMR experiments were also taken into account, and possible unit cell dimensions were determined. The best unit cell was selected that was also consistent with other data.

Calculation of Diffraction Patterns. Fiber diffraction patterns were generated from a range of model coordinates contained within an orthogonal unit cell containing two pairs of β-strands in different arrangements including the AP arrangement (with dimensions) 9.32 × 18.5 × 40.3 Å^3. The geometry of a fiber was taken into account, and the fiber axis was defined as parallel to the hydrogen bonding direction.[33,34] Calculated diffraction patterns were compared with the experimental diffraction pattern by overlaying the two patterns and examining close matches between the experimental and calculated diffraction signal positions.

Results and Discussion

Characterization of Fibril Morphology. A procedure was first established for preparing hIAPP$_{20-29}$ fibrils suitable for structural analysis by SSNMR. The peptide forms a gel-like precipitate consisting of unbranched fibrils with the characteristics of amyloid, being ∼10 nm in diameter and several hundred nanometers long (Figure 1a). The ^{13}C CP-MAS NMR spectrum of a frozen solution of monomeric [U-^{13}C,^{15}N-FGAI]hIAPP$_{20-29}$ shows single peaks for each carbon site (Supporting Information, Figure S1), but a ^{13}C DARR spectrum of fibrils formed by the same peptide shows duplication of the peaks for some of the amino acid sites (Figure 1b). The fibrils thus appear morphologically homogeneous by electron microscopy, but the ^{13}C

(24) Bennett, A. E.; Rienstra, C. M.; Auger, M.; Lakshmi, K. V.; Griffin, R. G. *J. Chem. Phys.* **1995**, *103*, 6951.
(25) Antzutkin, O. N.; Tycko, R. *J. Chem. Phys.* **1999**, *110*, 2749.
(26) Takegoshi, K.; Nakamura, S.; Terao, T. *Chem. Phys. Lett.* **2001**, *344*, 631.
(27) Jaroniec, C. P.; MacPhee, C. E.; Astrof, N. S.; Dobson, C. M.; Griffin, R. G. *Proc. Natl. Acad. Sci. U.S.A.* **2002**, *99*, 16748.
(28) Cornilescu, G.; Delaglio, F.; Bax, A. *J. Biomol. NMR* **1999**, *13*, 289.
(29) Hong, M.; Gross, J. D.; Griffin, R. G. *J. Phys. Chem.* **1997**, *101*, 5869.
(30) Costa, P. R.; Gross, J. D.; Hong, M.; Griffin, R. G. *Chem. Phys. Lett.* **1997**, *280*, 95.
(31) Pan, Y.; Gullion, T.; Schaefer, J. *J. Magn. Reson.* **1990**, *90*, 330.
(32) Levitt, M. H.; Raleigh, D. P.; Creuzet, F.; Griffin, R. G. *J. Chem. Phys.* **1990**, *92*, 6347.
(33) Makin, O. S.; Serpell, L. C. In *Amyloid proteins: methods and protocols*; Sigurdsson, E. M., Ed.; Humana press: Totowa, NJ, 2005; pp 67−80.
(34) Makin, O. S.; Sikorski, P.; Serpell, L. C. *J. Appl. Crystallogr.* **2007**, *40*, 966.

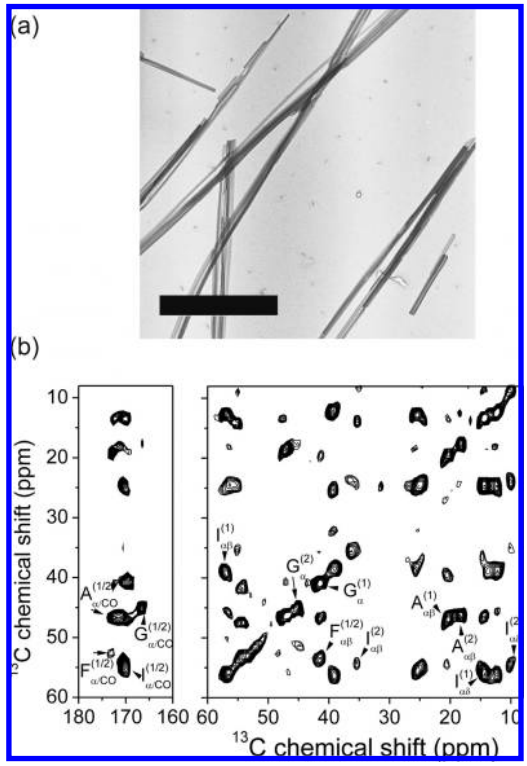

Figure 1. Analysis of the polymorphism of hIAPP peptide aggregates. (a) Negative stain electron micrographs of $hIAPP_{20-29}$ aggregates prepared without seeding (scale bar = 200 nm). (b) Two-dimensional ^{13}C DARR NMR spectrum of hydrated fibrils of [U-^{13}C,^{15}N-FGAI]$hIAPP_{20-29}$ obtained with a mixing time of 50 ms. Fibrils were prepared by incubation of the peptide solution at 37 °C without seeding. Superscripts refer to fibril forms (1) and (2).

spectrum implies that at the molecular level the fibrils consist of two structurally distinct forms. The two forms could occur either within separate protofilaments or within domains within each protofilament. By integrating all the clearly doubled peaks for the two forms, it was estimated that the major form, denoted (1), was present in between a 1.5- and 2-fold excess over the minor form, denoted (2). The slight excess of form (1) was reproduced each time fibrils were grown under these conditions, even from different batches of peptide.

Backbone and Cβ ^{13}C chemical shifts for forms (1) and (2) are documented in Table 2. Peaks for residues F, G, A, and I show clear duplication, but structure prediction from the chemical shift values using TALOS[28] suggests that the backbone ϕ and ψ angles for both fibril forms fall within the acceptable limits for a β-strand geometry extending along the entire peptide (Table 3). The possibility of other structures cannot be ruled out from chemical shift analysis alone, however.

Alignment of Peptide Molecules. We investigated the possibility that the duplication of chemical shifts for $hIAPP_{20-29}$ arose from differences in the alignment of hydrogen-bonded β-strands within forms (1) and (2). Neighboring strands could, for example, have a parallel alignment in one form and antiparallel in the other and may be in-register or out-of-register. The peptide alignment within the two forms was examined using rotational resonance (RR) NMR[35,36] to estimate distance-dependent intermolecular ^{13}C dipolar couplings between specific sites of hydrogen bonded peptides. Weak dipolar couplings between ^{13}C spins are normally averaged to zero by sample rotation at the magic angle but are reintroduced when an RR condition is met. By preparing an initial state of longitudinal

Table 2. Summary of ^{13}C Chemical Shift Values for the Carbonyl (C′), α, and β Positions for the Two Forms (1) and (2) of Unseeded $hIAPP_{20-29}$ Fibrils[a]

	chemical shift (ppm)		
res.	C′	Cα	Cβ
S20	167.93	54.44	60.99
N21	171.44	49.70	39.37
N22	170.57	49.70	39.37
F23	173.77 (170.22)	53.62 (51.93)	41.41
G24	166.65 (168.37)	41.21 (45.15)	-
A25	171.45 (170.40)	46.98 (46.20)	19.92 (18.86)
I26	171.22 (171.41)	57.66 (54.85)	39.10 (35.17)
L27	172.95	51.14	42.49
S28	172.54	52.99	63.65
S29	177.50	56.40	65.90

[a] Where clear peak duplication occurs, values for form (2) are shown in parentheses. Most values were measured from ^{13}C DARR spectra of [U-^{15}N,^{13}C-SNNF]$hIAPP_{20-29}$, [U-^{15}N,^{13}C-FGAI]$hIAPP_{20-29}$, and [U-^{15}N,-^{13}C-ILSS]$hIAPP_{20-29}$. Values for F23 (C′ and Cα) and I26 (C′) were measured from fibrils containing [U-$^{13}C\alpha$-F23]$hIAPP_{20-29}$ and [U-^{13}-C′-F23]$hIAPP_{20-29}$ or [U-$^{13}C'$-I26]$hIAPP_{20-29}$.

Table 3. Summary of Backbone Torsional Angles for Unseeded $hIAPP_{20-29}$ Fibril Form (1) and (2) Predicted from ^{13}C and ^{15}N Chemical Shifts Using TALOS[28]

	form (1)		form (2)	
res.	ϕ	ψ	ϕ	ψ
S20	–	–	–	–
N21	-121 ± 11	121 ± 8	-121 ± 11	121 ± 8
N22	-120 ± 8	129 ± 15	-120 ± 8	129 ± 15
F23	-135 ± 5	141 ± 15	-121 ± 11	140 ± 16
G24	-118 ± 13	136 ± 19	-133 ± 16	142 ± 17
A25	-125 ± 15	125 ± 11	-121 ± 17	131 ± 12
I26	-125 ± 13	126 ± 13	-97 ± 6	116 ± 15
L27	-112 ± 12	118 ± 11	-112 ± 12	118 ± 11
S28	-109 ± 9	136 ± 22	-109 ± 9	136 ± 22
S29	–	–	–	–

difference polarization, measurements of peak intensity variations over a range of mixing periods can be related to dipolar couplings between pairs of ^{13}C spins separated by up to ~6.0 Å. Fibrils prepared from mixtures of peptides labeled at either the Cα or C′ positions of appropriate amino acid residues can be examined at RR to obtain distance constraints on the strand alignment within β-sheets. The repeating distance between β-sheets, observed from fiber diffraction patterns of amyloid fibrils, is typically 9 Å or greater, and so the possibility of detecting intersheet Cα−C′ interactions by RR is very unlikely.

RR measurements were first performed on fibrils prepared from a mixture of [$^{13}C\alpha$-F23]$hIAPP_{20-29}$ and [$^{13}C'$-F23]-$hIAPP_{20-29}$ in a 5:1 molar ratio. The ^{13}C CP-MAS spectrum of the mixed fibrils (Figure 2a) shows a pair of peaks for the Cα labels, separated by 171 Hz, and a pair of peaks for the C′ labels, separated by 375 Hz. The lower-field peak of each pair, which is ~1.5 times greater in area than that of the higher-field peak, was assigned tentatively to form (1). The first-order ($n = 1$) RR condition is set by adjusting the sample spinning rate (ω_R) to the difference ($\Delta\Omega$) in the resonance frequencies for $^{13}C\alpha$ and $^{13}C'$ spins. Thus the $n = 1$ RR condition is 12 031 Hz for form (1) and 11 827 Hz for form (2). Plots representing the time dependence of difference polarization were obtained after

(35) Thompson, L. K.; McDermott, A. E.; Raap, J.; Vanderwielen, C. M.; Lugtenburg, J.; Herzfeld, J.; Griffin, R. G. *Biochemistry* **1992**, *31*, 7931.
(36) Raleigh, D. P.; Levitt, M. H.; Griffin, R. G. *Chem. Phys. Lett.* **1988**, *146*, 71.

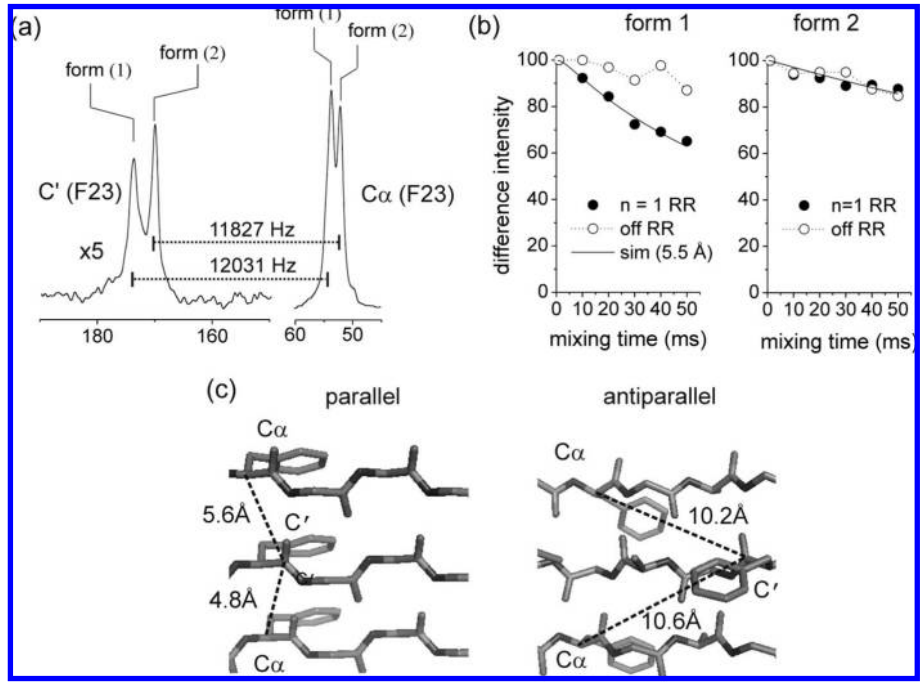

Figure 2. Determination of peptide alignment within $hIAPP_{20-29}$ form (1) and (2) from ^{13}C RR measurements on fibrils of 5:1 [α-^{13}C-F23]$hIAPP_{20-29}$/[C′-^{13}C-F23]$hIAPP_{20}$. (a) A ^{13}C CP-MAS NMR spectrum showing peaks for Cα and C′ of the two fibril forms and their frequencies of separation. (b) Peak intensity difference curves indicating the extent of magnetization exchange between specific Cα and C′ spin populations at $n = 1$ RR (●) for forms (1) and (2). Off RR control curves were obtained at a MAS rate of 13 kHz (○). Solid lines are simulated curves in closest agreement with the experimental data, corresponding to the $^{13}C-^{13}C$ distances shown. (c) Diagnostic F23 Cα−C′ distances in models of $hIAPP_{20-29}$ as in-register, parallel, and antiparallel alignments.

scaling the measured peak intensities to eliminate the background from the ∼70% of ^{13}Cα labeled peptides that are not hydrogen bonded to a C′ labeled peptide.

The plot of peak intensity difference for form (1) at $n = 1$ RR shows a steady decline at increasing mixing periods (Figure 2b, left, ●). Control plots measured from the same peaks off RR show very little time dependence (Figure 2b, left, ○). Moreover, difference intensities measured at MAS frequencies corresponding to the separation of the outermost peaks (12 202 Hz) or innermost peaks (11 656 Hz) were indistinguishable from the curves off-RR (data not presented). That Zeeman exchange occurs only at the spinning rate of 12 031 Hz confirms that the lowest field peaks for C′ and Cα correspond to the same fibril form. By comparing the experimental data at $n = 1$ RR with numerically simulated curves to produce a χ^2 matrix (Supporting Information Figure S2) the $^{13}C\alpha-^{13}C'$ distance for F23 in form (1) was estimated to be 5.5 Å, although the precision and accuracy of the distance calculation are subject to the assumptions made in the manipulation of the peak intensity values to eliminate background contributions. The ability to distinguish Zeeman exchange from the natural decay of peak intensities that occurs off-RR nevertheless indicates that the $^{13}C\alpha-^{13}C'$ distance is less than 6.0 Å, which is generally considered to be the upper limit of detection for $^{13}C-^{13}C$ distances. For form (2), the peak intensity difference plot at $n = 1$ RR (11827 Hz) is virtually indistinguishable from the off-RR control curve, indicating that the $^{13}C\alpha-^{13}C'$ distance is likely to be greater than 6.0 Å (Figure 2b, right).

Models of the peptide show that if hydrogen-bonded strands are aligned parallel to one another and in-register (i.e., with each residue of a strand hydrogen bonded to the same residue of neighboring strands), the intermolecular $^{13}C\alpha-^{13}C'$ distance for F23 is less than 5.6 Å, whereas the distance for an in-register antiparallel arrangement is ∼10 Å (Figure 2c). The data for form (1) are thus consistent with a parallel alignment, although the distances measured are not precise enough to distinguish in-register strands from strands that are ±1 residue out-of-register (i.e., with F23 hydrogen bonded to N22 or G24 of neighboring peptides). The data for form (2) are consistent with either a parallel alignment that is 2 or more residues out-of-register or an antiparallel alignment.

The strand alignment in form (2) was investigated further by RR analysis of fibrils grown from [$^{13}C\alpha$-F23]$hIAPP_{20-29}$ and [$^{13}C'$-I26]$hIAPP_{20-29}$ in a 5:1 molar ratio. The ^{13}C CP-MAS spectrum showed two partially resolved peaks for Cα of F23 in the two forms, but the peaks for C′ of I26 coincided for the two forms (Figure 3a). Sample spinning rates of 11 872 and 11 713 Hz were needed to match the exact $n = 1$ RR condition for each form, and assumptions had to be made about the relative contributions of the two forms to the C′ peak intensity (i.e., 1.5:1). Peak intensity difference curves for form (1) on and off RR were virtually indistinguishable from each other, consistent with a $^{13}C\alpha-^{13}C'$ distance of >6.0 Å between F23 and I26 of neighboring strands (Figure 3b, left). For form (2), the data at $n = 1$ RR are consistent with a distance of 4.9 Å (Figure 3b, right), which is strong evidence that the strands adopt an antiparallel arrangement in this form. For antiparallel strands in an in-register alignment the predicted distance is between 4.5 and 5.5 Å (Figure 3d).

Additional evidence that the fibrils contain a form having an antiparallel alignment was provided by a two-dimensional ^{13}C DARR experiment on fibrils grown from [U-^{13}C,^{15}N-N21/S28]$hIAPP_{20-29}$ (Figure 3c). Cross-peaks occurring between Cβ of N21 and Cβ of S28 are consistent with an intraresidue $^{13}C-^{13}C$ distance of <6.0 Å, which can occur for in-register antiparallel strands (for which the predicted distance is ∼4.7

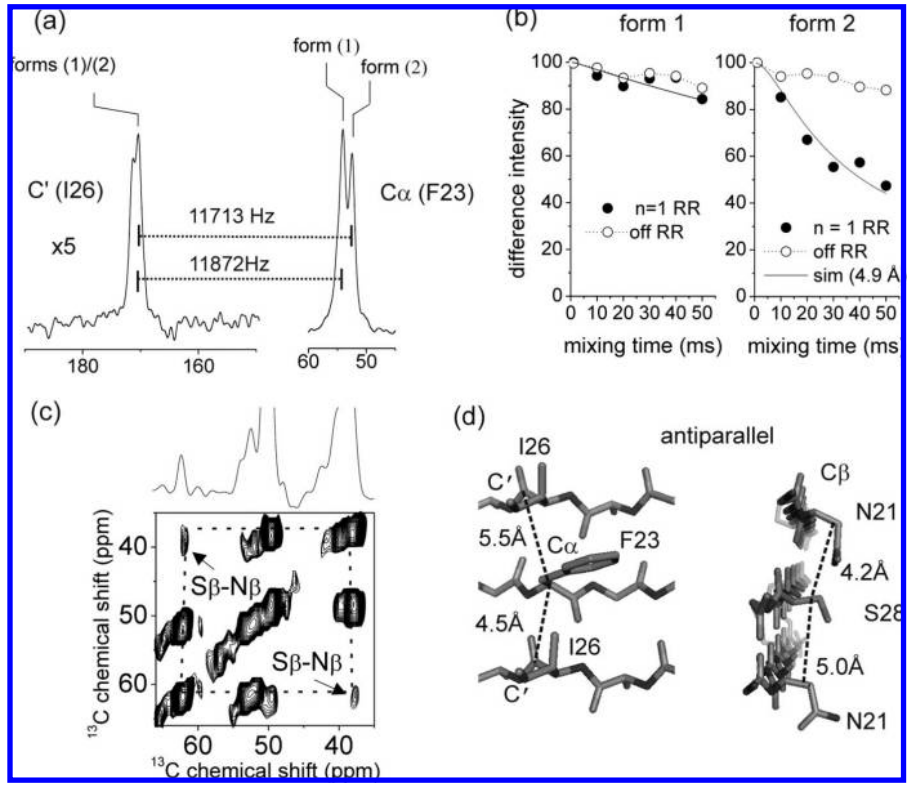

Figure 3. Determination of peptide alignment within $hIAPP_{20-29}$ form (2). (a) A ^{13}C CP-MAS NMR spectrum of fibrils of 5:1 [$^{13}C\alpha$-F23]$hIAPP_{20-29}$/[$^{13}C'$−I26]$hIAPP_{20-29}$ showing the two partially resolved peaks for Cα of F23 and the overlapped peaks for C′ of I26. (b) Magnetization exchange curves at $n = 1$ RR for forms (1) and (2). Solid lines are numerically simulated curves in close agreement with the data, corresponding to $^{13}C-^{13}C$ distances where shown. (c) A 2D ^{13}C DARR spectrum of fibrils grown from [U-^{13}C,^{15}N-N21/S28]$hIAPP_{20-29}$, highlighting cross-peaks between the N21/S28 β-carbons, consistent with a $^{13}C-^{13}C$ distance of less than 6 Å. The spectrum was obtained at an MAS rate of 8 kHz with a 200-ms mixing time and is the result of accumulating 1024 scans for each of 64 increments in t_1. Above the spectrum is a horizontal cross section at the frequency of N21 Cβ (38 ppm), showing cross-peak intensity at the frequency of S28 Cβ (61 ppm). (d) The relationship between the Cα−C′ distance constraints and peptide alignment for an in-register antiparallel configuration.

Å) but not for parallel strands (for which the predicted distance is ∼22 Å)(Figure 3d). It is not possible to assign the cross-peaks specifically to either form (1) or (2), but taken together with the RR data, it is reasonable to suggest that coupling between N21 and S28 originates from form (2).

Concluding this section, SSNMR measurements have shown that $hIAPP_{20-29}$ fibrils contain two forms, one having parallel and the other antiparallel strands, which may originate from separate protofilaments or from domains within individual protofilaments.

Selection of Single Fibril Morphology. For further structural characterization of form (1) and (2) it was necessary to isolate one or both of the forms. Single fibril morphologies can, in principle, be produced by self-seeding or cross-seeding with sonciated preformed fibrils that are morphologically pure. For example, Aβ_{1-40} fibril fragments have been used to seed the growth of Aβ_{10-40} fibrils to propagate fibril morphology and molecular structure.[13] Full-length amylin has a high propensity to form polymorphic amyloid fibrils[37] and so was considered here as unsuitable as a seed for selecting a unique $hIAPP_{20-29}$ fibril morphology. Seeds were prepared instead from an unlabeled amylin variant $hIAPP_{8-37}$, obtained by truncating the N-terminal disulphide region (Figure S3 of Supporting Information), which consistently formed morphologically homogeneous,

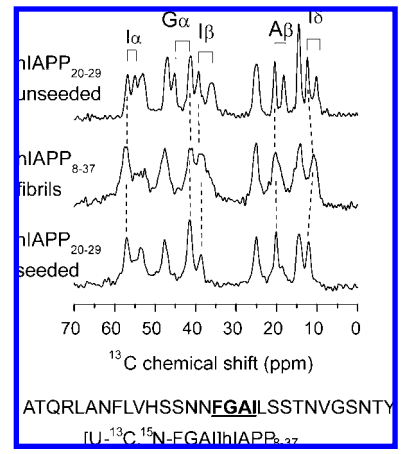

Figure 4. ^{13}C CP-MAS NMR experiments to compare the polymorphism of unseeded $hIAPP_{20-29}$ fibrils and $hIAPP_{20-29}$ fibrils obtained by seeding with sonicated $hIAPP_{8-37}$ fibrils. Spectra are shown for (from top to bottom) unseeded [U-^{13}C,^{15}N-FGAI]hIAPP fibrils, unsonicated [U-^{13}C,^{15}N-FGAI]h-$IAPP_{8-37}$ fibrils, and [U−^{13}C,^{15}N-FGAI]$hIAPP_{20-29}$ fibrils isolated immediately after seeding with sonicated unlabeled $hIAPP_{8-37}$ fibrils. The MAS rate was 8 kHz.

long, and unbranched fibrils (data not presented). The ^{13}C CP-MAS NMR spectrum of [U-^{13}C,^{15}N-FGAI]$hIAPP_{8-37}$ fibrils shows only single peaks for each ^{13}C site, consistent with only one molecular structure within the fibrils (Figure 4, middle). Insoluble $hIAPP_{20-29}$ fibrils formed instantaneously in a 75% yield by cross-seeding with sonicated fibrils of $hIAPP_{8-37}$. The

(37) Goldsbury, C. S.; Cooper, G. J. S.; Goldie, K. N.; Muller, S. A.; Saafi, E. L.; Gruijters, W. T. M.; Misur, M. P. *J. Struct. Biol.* **1997**, *119*, 17.

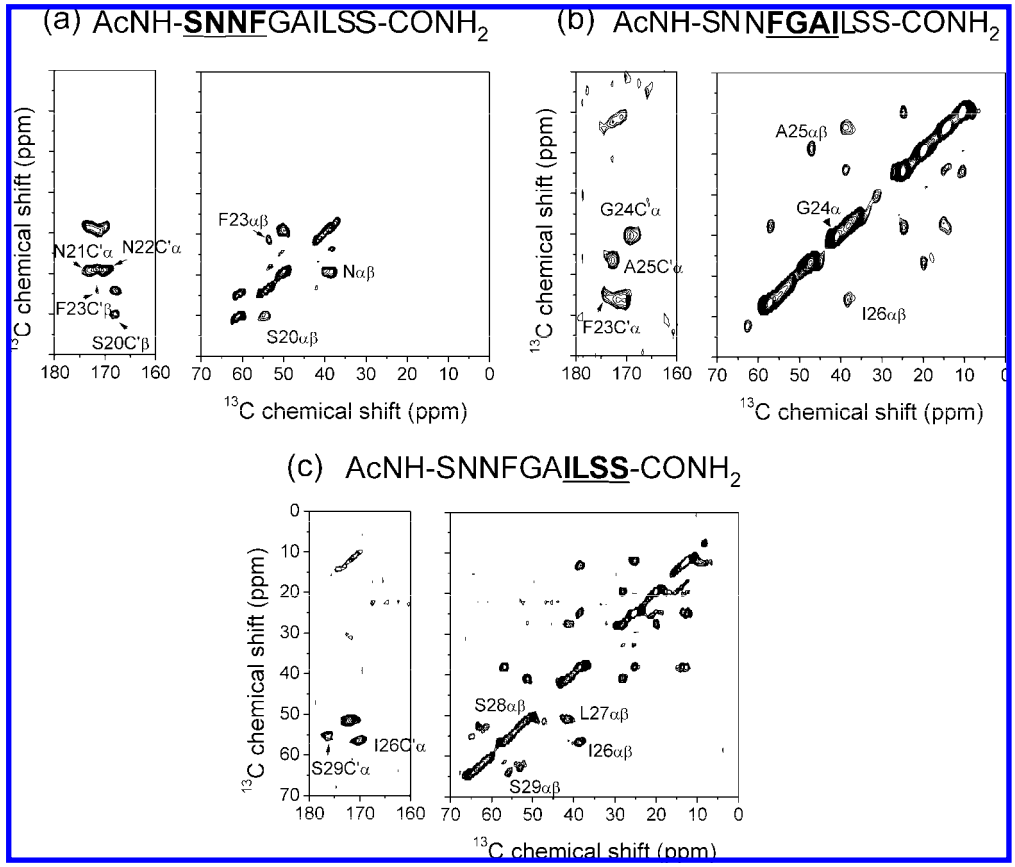

Figure 5. ^{13}C DARR NMR spectra of seeded fibrils of block-^{13}C/^{15}N labeled hIAPP$_{20-29}$. Spectra are shown for (a) [U-^{13}C,^{15}N-SNNF]hIAPP$_{20-29}$, (b) [U-^{13}C,^{15}N-FGAI]hIAPP$_{20-29}$, and (c) [U-^{13}C,^{15}N-ILSS]hIAPP$_{20-29}$. All samples were prepared by seeding with sonicated fibrils of hIAPP$_{8-37}$. Spectra were obtained with a 1-ms mixing time and are the result of accumulating 128 scans for each t_1 increment.

^{13}C CP-MAS NMR spectrum of seeded [U-^{13}C,^{15}N-FGAI]hIAPP$_{20-29}$ fibrils shows single peaks for each site (Figure 4, bottom), at remarkably similar positions to the peaks for [U-^{13}C,^{15}N-FGAI]hIAPP$_{8-37}$ fibrils. The ^{13}C DARR spectra of seeded fibrils of [U-^{13}C,^{15}N-SNNF]hIAPP$_{20-29}$, [U-^{13}C,^{15}N-FGAI]hIAPP$_{20-29}$, and [U-^{13}C,^{15}N-ILSS]hIAPP$_{20-29}$ are shown in Figure 5. All the backbone and Cβ ^{13}C chemical shift values for the 10 residues of the seeded fibrils (Table S1 of the Supporting Information) lie within ±0.5 ppm of those measured for form (1) of [U-^{13}C,^{15}N-FGAI]hIAPP$_{20-29}$ in the unseeded fibrils, suggesting that the structures of the seeded fibrils and unseeded form (1) are similar or identical. Extensive structural measurements will be required to confirm the architectural similarity of the seeded and unseeded fibrils, however, and so it cannot be ruled out at this stage that the seeded fibrils adopt a third structure that is distinct from both form (1) and (2), but which has similar NMR properties to form (1).

Structural Analysis of Seeded Fibrils. A total of 38 ^{13}C/^{15}N chemical shift values were obtained from the DARR spectra (Figure 5) and HETCOR spectra (Table S1 and Figure S4a and S4b in the Supporting Information). Backbone ϕ/ψ torsional angles were estimated from chemical shifts[28] and are summarized in Table 4. Further constraints on the ϕ/ψ torsional angles were obtained for F23, A25, I26, L27, and S28 using methods to measure relative N−H and C−H bond orientations (Figure S4c and S4d in the Supporting Information). All the torsional angle measurements and predictions were consistent with the peptide within the seeded fibrils adopting an unbroken β-strand involving all 10 residues, ~36 Å in length. This structure contrasts with the crystal structure of the peptide

Table 4. Summary of Backbone Torsional Angles for Seeded hIAPP$_{20-29}$ Fibrils Predicted from ^{13}C and ^{15}N Chemical Shifts (TALOS) and Measured Directly As Absolute Values

	TALOS		direct	
res.	ϕ	ψ	ϕ	ψ
S20	–	–	–	–
N21	−111 ± 9	117 ± 5	–	–
N22	−117 ± 16	129 ± 10	–	–
F23	−126 ± 9	144 ± 10	−130 ± 10	140 ± 15
G24	−123 ± 17	139 ± 19	–	–
A25	−117 ± 17	130 ± 11	−135 ± 15	140 ± 15
I26	−119 ± 20	139 ± 13	−150 ± 15	150 ± 10
L27	−120 ± 11	131 ± 23	−150 ± 10	140 ± 10
S28	−111 ± 22	134 ± 19	−150 ± 15	150 ± 10
S29	–	–	–	150 ± 10

NNFGAIL, which has a pronounced bend around F23 and G24 facilitating a tight main chain−main chain interface.[19] No evidence was found here for the significant angular deviations from a β-strand geometry that would be required to create a similar bend in hIAPP$_{20-29}$.

The torsional angles (χ_1, χ_2) defining the I26 side chain conformation were estimated from analysis of dephasing curves measured in a ^{13}C-detect, ^{15}N-dephase REDOR experiment (Figure 6). The experimentally dephased signal (S_D) for Cγ and Cδ at different dephasing intervals was compared with simulated dephasing curves for a three-spin system incorporating the backbone ^{15}N and Cγ or Cδ for the residue i of interest (N_i, Cδ, Cγ) and ^{15}N for residue $i+1$ (N_{i+1}).[38] The simulations took into consideration the individual N_i−C and N_{i+1}−C distances and the angle N_i−C−N_{i+1} but assumed that N_i−N_{i+1}

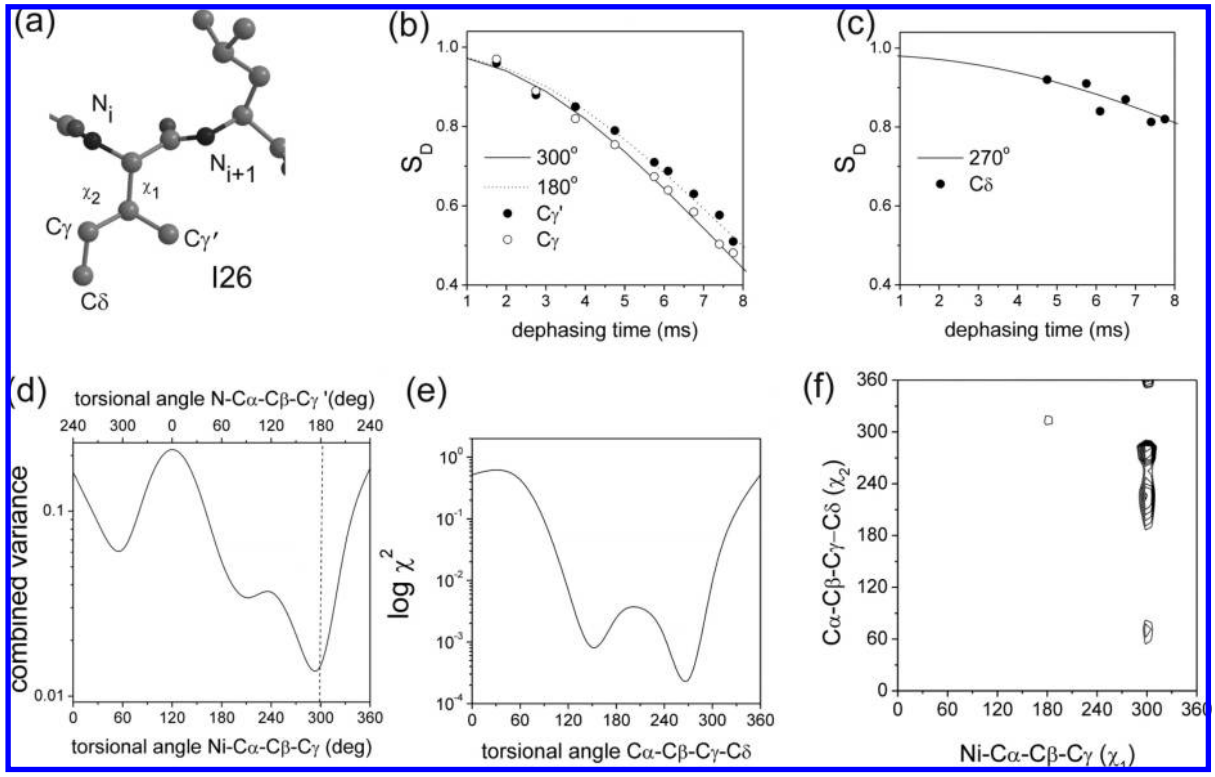

Figure 6. Experiments to estimate the side chain conformation of I26 within seeded [U-^{13}C,^{15}N-ILSS]hIAPP$_{20-29}$ fibrils. (a) Torsional angles χ_1 and χ_2 were measured by monitoring rotational echo double resonance (REDOR) dephasing of signals for Cγ, Cγ', and Cδ by N_i and N_{i+1}. (b) Experimental REDOR curves for dephasing of Cγ and Cγ' signals (symbols) and best fitting simulated curves (lines). The simulated curves correspond to a N−Cα−Cβ−Cγ (χ_1) angle of 300° (i.e., −60°) and a N−Cα−Cβ−Cγ' angle of 180°. (c) REDOR curve for dephasing of the Cδ signal showing the best fitting curve for a χ_2 angle of 270°. (d) A plot of the variance of the combined Cγ and Cγ' dephasing data from simulated REDOR curves for different N−Cα−Cβ−Cγ (χ_1)/N−Cα−Cβ−Cγ' combinations, showing the minimum variance at 300°/180°. (e) A variance plot for the REDOR measurements of χ_2, maintaining angle χ_1 at a fixed value of 300°. (f) A contour plot showing the χ_1/χ_2 angles in closest agreement with the experimental data.

couplings were negligible as justified previously.[39] The backbone geometry separating N_i and N_{i+1} was based on standard peptide bond lengths and angles, and the median torsional angles ϕ and ψ were taken from the range measured for residues Ile and Leu using the N−C−C−N and H−N−C−H experiments. The calculated curves in closest agreement with the experimental data corresponded to a χ_1 angle of −60° (i.e., a gauche (−) conformation) and a χ_2 angle of 270° (Figure 6). The effect of ^{13}C−^{13}C couplings on the dephasing curves, particularly at dephasing times over 5 ms, were not taken into consideration, and thus the angle values must be regarded only as estimates. Similar measurements for L27 (Figure S5 of the Supporting Information) yielded χ_1 and χ_2 values of ±30° and 90°, respectively. It was not possible to measure angles for N21, N22, and F23 because of uncertainties in the simulation parameters and in the peak assignments for the F23 aromatic ring.

Strand Alignment in Seeded Fibrils. Experiments were carried out to establish whether the seeded fibrils contained parallel strands as in form (1) or antiparallel strands as in form (2). A ^{13}C DARR experiment on seeded fibrils grown from [U-^{13}C,^{15}N-N21/S28]hIAPP$_{20-29}$ (Figure 7a) lacks the cross-peaks between Cβ of N21 and Cβ of S28 observed for the unseeded fibrils (Figure 3c), suggesting that the fibrils did not have the same antiparallel strand arrangement observed in the unseeded fibrils. An RR experiment on seeded fibrils of [^{13}Cα-F23]hIAPP$_{20-29}$ and [^{13}C′-F23]hIAPP$_{20-29}$ in a 5:1 molar ratio shows polarization exchange consistent with an interstrand ^{13}C−^{13}C distance of ∼5.4 Å (Figure 7b and c) and diagnostic of a parallel strand arrangement as shown in Figure 2c. The strand alignment was probed further in a multiple quantum (MQ) NMR experiment on seeded fibrils of [β-^{13}C-A]hIAPP$_{20-29}$. The coherence orders excited represent the number of spins that are correlated through a dipolar-coupling network and can report on the supramolecular structure of fibrils by identifying clusters of groups or molecules. Here up to 8 orders of quanta were detected, indicating that the β-methyl groups of at least 8 peptide strands were coupled to each other and thus separated by a repeat distance of less than 6 Å (Figure 7d). If the strands were parallel but out-of-register by one ± 1 amino acid (i.e., A25 of one strand is hydrogen bonded to G24 or I26 of a neighbor) the β-methyl groups would be situated on opposite faces of the β-sheet layer and the repeating distance between them would exceed 6 Å. Together, these results are consistent with the seeded fibrils having a parallel strand arrangement, as occurs for form (1), and with an in-register alignment.

Determination of the Cross-β Spine Architecture. Recent studies of microcrystals of short amyloidogenic peptide fragments suggest a common cross-β spine consisting of a pair of β-sheets separated by ∼10 Å. In most cases so far examined by crystallography, the layers are packed together with interdigitated side groups forming a steric zipper.[2,3] The spine can be either parallel or antiparallel *within* each β-sheet strand, as observed for the two unseeded hIAPP$_{20-29}$ forms and also parallel or antiparallel *between* each sheet (i.e., AP, AA, PA,

(38) Goetz, J. M.; Schaefer, J. *J. Magn. Reson.* **1997**, *127*, 147.
(39) Balbach, J. J.; Yang, J.; Weliky, D. P.; Steinbach, P. J.; Tugarinov, V.; Anglister, J.; Tycko, R. *J. Biomol. NMR* **2000**, *16*, 313.

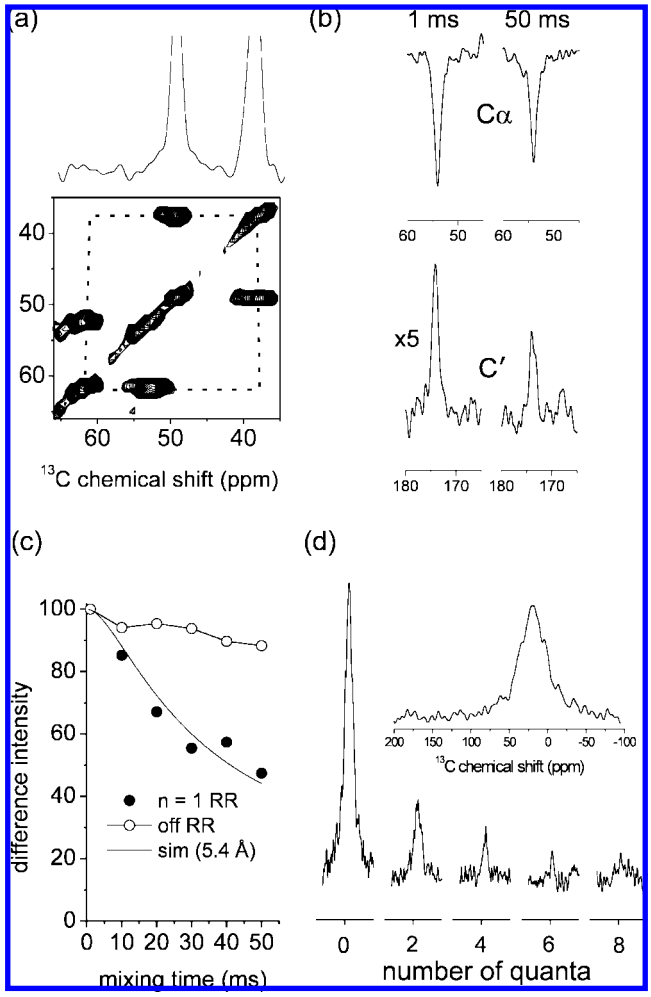

Figure 7. Experiments to investigate the alignment of β-strands in hIAPP$_{20-29}$ fibrils prepared by seeding with sonicated fibrils of hIAPP$_{8-37}$. (a) A spectrum of seeded fibrils prepared from [U-^{13}C,^{15}N−N21/S28]hIAPP$_{20-29}$. The spectrum was obtained as described in Figure 3. The horizontal cross section shows no cross-peak intensity at the frequency of S28 Cβ. (b) Representative spectra from a RR experiment on seeded fibrils of 5:1 [^{13}Cα-F23]hIAPP$_{20-29}$/[13C′-F23]hIAPP$_{20}$, showing peaks for Cα (inverted) and C′ at mixing periods of 1 and 50 ms. (c) Time dependence of peak difference intensities at $n = 1$ RR and off RR. The solid line shows a simulated curve in closest agreement with the data at $n = 1$ RR. (d) Static ^{13}C MQ excitation spectra of seeded fibrils of [^{13}Cβ-A25]hIAPP$_{20-29}$ at a preparation/mixing time of 14.4 ms.

and PP) as defined in Figure 8a. Assuming that hIAPP$_{20-29}$ in all its forms conforms to a typical steric zipper type configuration, the seeded fibrils and the unseeded form (1) adopt either the PA or PP configuration and form (2) adopts either the AP or AA configuration.

To investigate the orientation of strands within and between the β-sheets of seeded hIAPP$_{20-29}$ fibrils in more detail, the seeded fibrils were examined further using X-ray fiber diffraction. An X-ray fiber diffraction pattern for the seeded fibrils (Figure 8b(i)) is consistent with parallel β-strands giving a characteristic diffraction signal at 4.7 Å. An antiparallel arrangement may give rise to a layer line at 9.4 Å, as shown in the calculated pattern in Figure 8b(ii), but this is not observed in the experimental pattern. A possible unit cell was determined from the diffraction signal positions (summarized in Table 5) and gave dimensions of $a = 4.7$ Å, $b = 18.5$ Å, $c = 40.3$ Å ($\alpha = \beta = \gamma = 90°$). The sheet distance repeat (b) is 18.5 Å and, therefore, expected to contain two peptides (giving a sheet

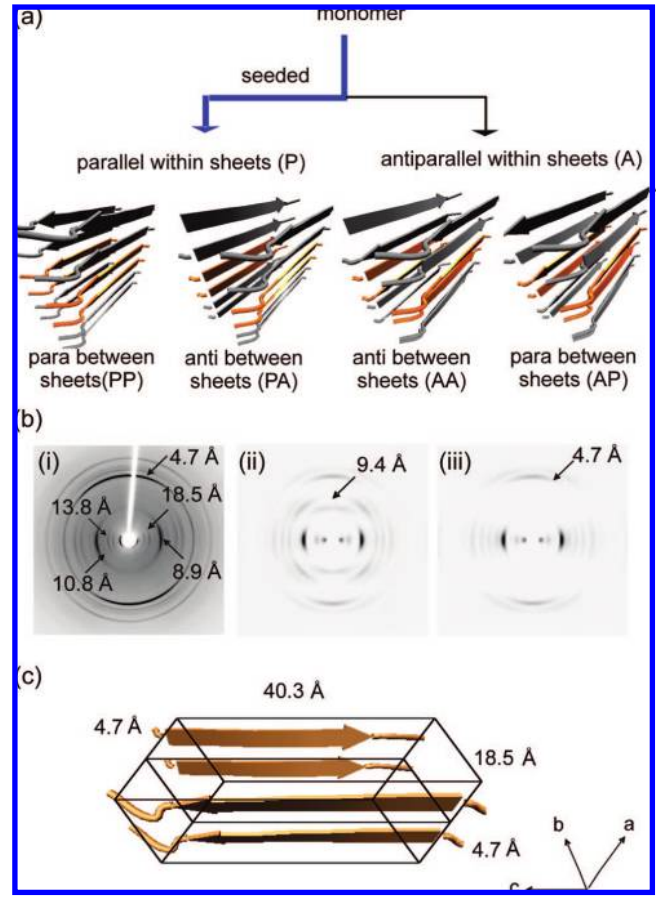

Figure 8. Polypeptide arrangements within a cross-β spine consisting of two β-sheet layers of in-register strands. (a) SSNMR demonstrates that a mixture of parallel and antiparallel arrangements within the β-sheets of each protofilament occurs in unseeded fibrils of hIAPP$_{20-29}$, while seeding with sonicated fibrils of hIAPP$_{8-37}$ results only in the parallel arrangement within the β-sheets. (b) X-ray fiber diffraction pattern for the seeded fibrils of hIAPP$_{20-29}$ with key reflection positions labeled (i), compared with calculated diffraction patterns for antiparallel (ii) and parallel (iii) β-strands within two β-sheets in a PA arrangement. (c) Unit cell dimensions and β-spine organization (in a PA arrangement) most consistent with the measured diffraction pattern in (b(i)) (*a* is the hydrogen bonding distance along the fiber axis, *c* is the peptide length, and *b* is the intersheet spacing).

Table 5. Measured Positions of Equatorial Reflections from the Experimental Diffraction Pattern Given by hIAPP(20−29) Fibrils with the Calculated Positions and Indexing from the Determined Unit Cell ($a = 4.66$ Å, $b = 18.47$ Å, $c = 40.3$ Å, $\alpha = \beta = \gamma = 90°$), Where *a* Is Parallel to the Fibre Axis Hydrogen Bonding Direction

observed diffraction signal positions (Å)	calculated diffraction signal positions (Å)	*h*	*k*	*l*
∼37	40	0	0	1
17.97	18.47	0	0	2
13.76	13.60	0	0	3
10.80	10.85	0	1	3
8.94	9.00	0	2	1
7.38	7.37	0	1	5
6.17	6.16	0	3	0

spacing of 18.5/2 = 9.2 Å). The peptide arrangement therefore conforms to the PA model, since the repeat distance for a PP model would be 9.3 Å, and this is not consistent with diffraction data. Model structures of the fibrils in a PA arrangement with different sheet spacings and angles arising from the SSNMR data were examined by calculating the diffraction patterns within the determined unit cell. The calculated patterns were then

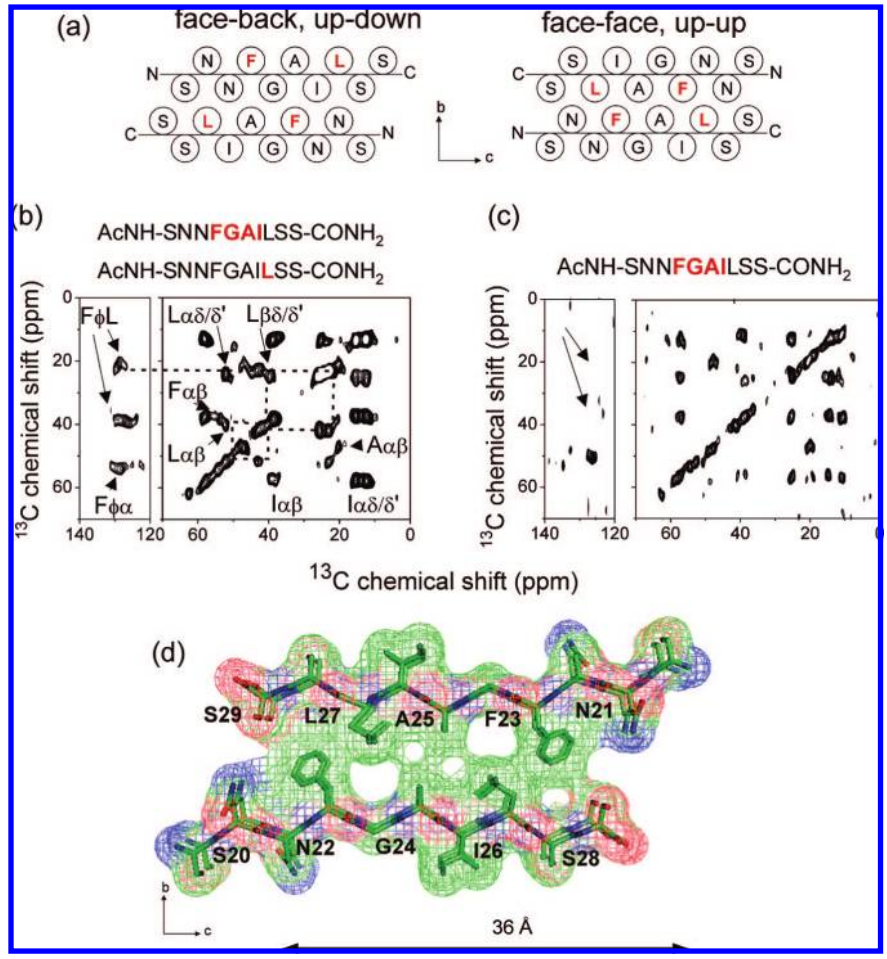

Figure 9. Experiments to identify the steric zipper arrangement of seeded fibrils of $hIAPP_{20-29}$. a) The two possible steric zipper arrangements of the β-spine showing the relative positions of F23 and L27 residues (labeled red). b) The DARR NMR spectrum of 1:1 [U-^{13}C,^{15}N-FGAI]$hIAPP_{20-29}$/[U-^{13}C,^{15}N-L27]$hIAPP_{20-29}$ fibrils shows cross peaks consistent with dipolar couplings between the aromatic carbons of F23 (Fϕ) and Cδ/Cδ' of L27. c) The F23-L27 cross-peaks are absent from the spectrum of [U-^{13}C,^{15}N-FGAI]$hIAPP_{20-29}$ fibrils alone. Spectra were obtained with a mixing time of 50 ms. d) Models of the steric zipper arrangement of the β-spine within seeded $hIAPP_{20-29}$ fibrils based on extensive SSNMR constraints and X-ray fiber diffraction data.

compared to experimental diffraction patterns to validate the models (Figure 8b(ii and iii)). From the models examined, Figure 8c shows a low resolution representation of the arrangement giving a calculated diffraction pattern with diffraction peaks most similar to those observed in Figure 8b(i).

The PA model in Figure 8c can adopt two principal configurations in which different faces of the peptide constitute the steric zipper[2,3] (Figure 9a). These configurations cannot be easily distinguished by X-ray fiber diffraction, but SSNMR dipolar coupling measurements can, in principle, distinguish between the two arrangements by providing constraints on close contacts between pairs of amino acid side groups from the two sheets. For example, positions within the L27 side groups of one sheet and the F23 side groups of the other may be close enough (<6 Å) to give rise to observable ^{13}C−^{13}C cross-peaks in a DARR NMR spectrum when the zipper adopts the face-to-face, up−up arrangement[2,3] (shown in Figure 9a, right). The two side groups are situated much further apart in a face-to-back, up−down arrangement (Figure 9a, left) and would not give rise to observable L27-F23 cross-peaks. To detect structurally diagnostic intermolecular couplings between the L27 side groups and F23, G24, A25, and I26, a DARR NMR spectrum was obtained from seeded fibrils formed by a 1:1 mixture of [U-^{13}C,^{15}N-FGAI]$hIAPP_{20-29}$ and [U-^{13}C,^{15}N-L27]$hIAPP_{20-29}$. The spectrum shows three strong cross-peaks between the F23 aromatic carbon (Fϕ) resonances at 130 ppm and resonances at 22, 40, and 55 ppm (Figure 9b). Two of these cross-peaks are consistent with intermolecular couplings between Fϕ and Lδ (or Lδ') (130−22 ppm) and Fϕ and Lβ (130−40 ppm). A control spectrum, obtained from fibrils of pure [U-^{13}C,^{15}N-FGAI]$hIAPP_{20-29}$ prepared under identical conditions to the mixed labeled fibrils, does not show the 130−22 ppm and 130−40 ppm cross-peaks (Figure 9c) indicating that the cross-peaks in the spectrum of the mixed labeled fibrils arise from intermolecular Fϕ-L couplings. Residues F23 and L27 are too far apart (>8.5 Å) within a single sheet to give rise to direct dipolar couplings, but the F23-L27 cross-peaks could arise indirectly from couplings between L27 and other residues which are relayed along the FGAI spin system during the DARR mixing period. Relay is unlikely here because there are few or no other interresidue cross-peaks that would signify such an effect. Hence the DARR spectrum is consistent with a β-spine having a face−face configuration (i.e., Figure 9a, right).

Figure 9d shows a model of the β-spine structure in the seeded fibril form (1), incorporating the I26 and L27 side chain conformations determined from SSNMR measurements and with the β-sheets staggered slightly to cover the 40 Å distance along c of the unit cell determined by X-ray fiber diffraction. The

exposed surface comprises polar side groups (S20, N22, S28), suggesting that the higher order fibril structure has wet and dry interfaces, akin to the observations in fibrils made of other small peptides.[2,3] The dry steric zipper is composed of predominantly hydrophobic contacts between the side chains of F23, A25, and L27, with the F23 aromatic groups forming a π-stacking column as implied by previous observations of impaired ring dynamics and short inter-ring distances.[23] Contacts between hydrophobic residues would help to stabilize the β-spine of form (1). An alternative model was also considered based on the NNFGAIL crystal structure, in which residues G, A, and I form a tight main chain−main chain interface rather than a typical steric zipper (Figure S6 of the Supporting Information). The peptide secondary structure in this model is not supported by the NMR measurements, but such an arrangement would maintain the close contact between residues F23 and L27 of the adjacent layers indicated by the NMR spectrum in Figure 9b. The unit cell dimensions for the alternative model did not conform to the dimensions determined from the diffraction pattern shown in Figure 8, and the calculated diffraction pattern was also somewhat different from the measured diffraction pattern. The combined NMR and diffraction measurements therefore allowed the alternative model to be ruled out.

Discussion

It is now known that the polymorphic (strain) behavior exhibited by prions[40,41] is a feature common to many fibrillogenic proteins and peptides, including Aβ_{1-40},[14] glucagon,[15] insulin,[10] amylin,[37] and α-synuclein.[7] Although fibrils generally share the same general elongated unbranched structure, morphological variations are often visible by electron microscopy and by spectroscopic observation. Polymorphism can arise from differences in the lateral association of individual protofilament units or, as is becoming increasingly apparent, as a consequence of variations in molecular conformation and packing within each protofilament. Goto and co-workers showed that, upon agitation, insulin forms simultaneously two distinct fibril types having different morphologies and distinct optical properties, which can self-propagate by seeding nonagitated insulin solutions.[42] Similarly an amyloidogenic fragment of β_2-microglobulin forms two types of fibrils differing in β-sheet content.[43] Here, SSNMR studies have shown that hIAPP$_{20-29}$ also simultaneously assembles into two types of fibril, or two domains within protofilaments. Unlike insulin and the β_2-microglobulin fragment, the two forms of hIAPP$_{20-29}$ are distinguished by the alignment of β-strands, one form having antiparallel strands and the other having parallel strands, which, to our knowledge, is the first example of such polymorphism to be verified experimentally. A similar parallel/antiparallel β-sheet configuration has been proposed to be responsible for glucagon fibril polymorphism, which occurs by varying growth conditions,[15] but this suggestion has not yet been confirmed by experimental measurements. It is not known at this stage whether the two forms correspond to distinct fibril or protofibril morphologies or to heterogeneity within each protofibril.

FTIR spectroscopic measurements of hIAPP$_{20-29}$ in unseeded fibrils provided an early crude model consisting of a uniform antiparallel strand configuration in which the central GAIL sequence is aligned with G24 hydrogen bonded to L27 of adjacent peptides.[21,22] In this model the aromatic rings of hydrogen bonded peptides would alternate between the two faces of each β-sheet layer. Our results do not support this arrangement in either of the two unseeded fibril forms, as the distance between Cα and C′ of F23 and I26 of adjacent peptides would be at least 2 Å longer than the distances estimated from our RR measurements (and greater than 6 Å, the upper limit of detection by RR). Subsequent SSNMR measurements by Lansbury and colleagues detected an intermolecular RR effect between Cα of A25 and C′ of I26, which was analyzed to produce a more complex refinement to the earlier crude antiparallel model.[21,22] RR effects between these two sites could also occur in principle in an antiparallel configuration with the sequence FGAI in registration (i.e., with F23 hydrogen bonded to I26 of adjacent strands). This alignment fits with the F23-I26 distance measured here for form (2) and all aromatic groups are situated on one face of the β-sheet. The spectra of the earlier study did not provide clear evidence for multiple fibril forms, however, although the line widths (~5 ppm) were somewhat broader than observed here, suggesting that structural heterogeneity or polymorphism may have been present in the fibrils that was not taken into consideration when translating the NMR measurements into a structural model.

It has been shown that the segment Aβ_{16-22} of the amyloid β-peptide is able to switch between parallel and antiparallel fibril arrangements, but only by chemical modification of the peptide to increase its amphiphilicity.[11] Here the simultaneous and spontaneous formation of the antiparallel and parallel β-sheet form for hIAPP$_{20-29}$ suggests similar energies of their formation and a stable molecular packing arrangement in both cases, perhaps as a consequence of both the parallel and antiparallel strands being able to form well packed hydrophobic cores. Further work will be required to investigate whether peptides of the general form P$_n$HGHHHP$_m$ (where P, H, and G are polar, hydrophobic, and glycine amino acids, respectively) are capable of forming polymorphic fibrils with different strand alignments. The stability given by hydrophobic contacts in form (1) could be preserved in form (2) of the unseeded fibrils if the antiparallel, hydrogen bonded strands within each sheet are arranged out-of-register such that all the F23 rings are facing inward toward the dry interface. Such an arrangement within any fibril has yet to be identified, and extensive experimental measurements will be necessary to provide a definitive model for form (2).

Fibril seeding of short peptide fragments by the parent polypeptide has been demonstrated for Aβ.[13] Here it is shown that a single fibril form of hIAPP$_{20-29}$ can be propagated selectively by heterologous seeding with hIAPP$_{8-37}$. Self-propagation of amyloid morphologies, or strain selection, occurs because the high fidelity of amyloid elongation rejects polymorphs dissimilar to the seeding species.[14,40,41] The cross-propagation observed here suggests that the seeded hIAPP$_{20-29}$ fibrils and the hIAPP$_{8-37}$ fibrils have related structural features at the molecular level. Indeed, the model for the seeded hIAPP$_{20-29}$ fibrils is also similar in some respects to the corresponding segment in the recent working model presented for full-length amylin,[8] having parallel β-strands with L27 and S29 forming the interface between two layers. The amylin model has a bend from residues 18−27, however, whereas our NMR and diffraction data indicate that hIAPP$_{20-29}$ is linear. This

(40) Tanaka, M.; Chien, P.; Yonekura, K.; Weissman, J. S. *Cell* **2005**, *121*, 49.
(41) Tanaka, M.; Chien, P.; Naber, N.; Cooke, R.; Weissman, J. S. *Nature* **2004**, *428*, 323.
(42) Dzwolak, W.; Loksztejn, A.; Galinska-Rakoczy, A.; Adachi, R.; Goto, Y.; Rupnicki, L. *J. Am. Chem. Soc.* **2007**, *129*, 7517.
(43) Yamaguchi, K.; Takahashi, S.; Kawai, T.; Naiki, H.; Goto, Y. *J. Mol. Biol.* **2005**, *352*, 952.

difference may result from the lack of flanking residues in the shorter peptide, which may influence the tertiary structure of full-length amylin or may simply be a consequence of the seeding fibrils, lacking the first 8 residues, having a different morphology to amylin. Although these residues may not play a direct role in fibrillization,[17,44] they do appear to modulate fibril growth and morphology. Removal of the disulphide reduces the ability of pre-existing $hIAPP_{8-37}$ fibrils to participate in the formation of new fibrils,[45] and full-length amylin fibrils contain three protofilaments whereas $hIAPP_{8-37}$ contains two protofilaments.[17]

The current $hIAPP_{20-29}$ model also differs from the crystal structure of the peptide NNFGAIL, which has a pronounced bend around the glycine residue. It should be noted, however, that the shorter peptides FGAIL and NFGAIL exhibit dissimilar fibril morphologies despite these peptides differing by only one amino acid.[20] Comparisons of our $hIAPP_{20-29}$ model with structures of other FGAIL-containing peptide segments of different length should therefore be treated with caution. Our model is supported by results from the Lansbury group, who interpreted differences in the lag times for $hIAPP_{20-29}$, and single and double mutations at F23 and S29 to argue that residues 23 and 29 interact with each other in the fibril assembly.[46] In our model the aromatic ring of F23 can be arranged so as to sit between L27 and S29 of an adjacent sheet layer, and this triad of residues may thus have important consequences for the rate of fibril growth, assembly of the cross-β spine, and the morphology of the mature fibrils (Figure 9d). Westermark and co-workers found that L23/P25 and P25/V26 variants of $hIAPP_{20-29}$ had reduced the fibril forming capacity under acidic conditions, supporting our argument that F23 and A25 contribute to the hydrophobic steric zipper that stabilizes the cross-β spine.[18] Similarly Raleigh and co-workers[47] used proline substitutions of $hIAPP_{20-29}$ to argue that residues at positions 22−28 are more important for fibril formation than the flanking residues 20, 21, and 29. Our model predicts that S20 and N21 are not essential for fibril formation, as the partial staggering of the two β-sheet layers excludes these residues from the stabilizing steric zipper region. Interestingly, the Westermark and Raleigh papers both identify S28 as being critical for fibril formation, as mutations at this position reduced the fibril forming capacity significantly. Our model places S28 on the opposite face to the steric zipper where one would expect less of a direct role of the serine side group in stabilizing the assembly. Interpretation of mutagenesis studies in terms of structural models should be done cautiously, however, because such studies do not shed light on which levels of fibril organization are destabilized by specific substitutions. Position 28, or indeed any of the positions, may influence interactions between protofibril intermediates or protofilaments rather than interactions within or between β-sheet layers. Moreover, substitutions that apparently do not affect fibril morphology may, in fact, have profound effects at the molecular level, as we have shown by comparing the ^{13}C NMR spectra and electron micrographs of the same sample (Figure 1).

Our earlier work indicates that the F23 rings are highly restrained and in close contact with one other, which implies that the rings are buried and stabilized by interactions with other side groups.[23] The current model places the F23 side groups close enough to one another to allow a network of $\pi-\pi$ interactions within each β-sheet layer but does not permit rings of different layers to interact with one another. Gazit has argued that $\pi-\pi$ interactions are essential for stabilizing fibril assemblies in peptides containing the FGAIL sequence.[48] Studies of full-length amylin by the Raleigh group found that the triple mutant F15L/F23L/Y37L forms amyloid fibrils of similar morphology to that of the wild-type polypeptide, suggesting that side-chain size and hydrophobicity at these positions may be more important than aromaticity for fibril assembly.[49] It is possible however that, by eliminating $\pi-\pi$ interactions, the fibrils simply adopt a new architecture that is more capable of accommodating different side group interactions.

In conclusion, the observation of distinct polymorphs involving both parallel and antiparallel structures formed from the same amino acid sequence highlights the opportunity for generating multiple amyloid folds with fundamentally different packing, but presumably similar conformational stability, from a single peptide sequence. Finally, the work presented here brings to the fore the power of SSNMR to identify and structurally characterize these different amyloid folds and serves as a platform from which to ascribe different amyloid structures to different phenotypic roles.

Acknowledgment. The UK Biotechnology and Biological Sciences are acknowledged for grant 36/B18704. LCS is supported by funding from BBSRC. S.E.R. was a BBSRC Professorial Fellow.

Supporting Information Available: Further details of numerical simulations, additional spectra, and electron micrographs. This material is available free of charge via the Internet at http://pubs.acs.org.

JA802483D

(44) Jaikaran, E.; Higham, C. E.; Serpell, L. C.; Zurdo, J.; Gross, M.; Clark, A.; Fraser, P. E. *J. Mol. Biol.* **2001**, *308*, 515.
(45) Koo, B. W.; Miranker, A. D. *Protein Sci.* **2005**, *14*, 231.
(46) Ashburn, T. T.; Lansbury, P. T. *J. Am. Chem. Soc.* **1993**, *115*, 11012.
(47) Moriarty, D. F.; Raleigh, D. P. *Biochemistry* **1999**, *38*, 1811.
(48) Gazit, E. *FASEB J.* **2002**, *16*, 77.
(49) Marek, P.; Abedini, A.; Song, B. B.; Kanungo, M.; Johnson, M. E.; Gupta, R.; Zaman, W.; Wong, S. S.; Raleigh, D. P. *Biochemistry* **2007**, *46*, 3255.